Dynamic contributions to the optical Stark effect in semiconductors

J. J. Baumberg, B. Huttner, R. A. Taylor, and J. F. Ryan
Department of Physics, Clarendon Laboratory, University of Oxford, Oxford OX1 3PU, United Kingdom
(Received 15 December 1992)

We present femtosecond time-resolved optical pump-probe measurements of the coherent excitonic nonlinear optical response in GaAs quantum wells. The data exhibit features that cannot be explained by the conventional description of the optical Stark effect as a rigid blueshift of the exciton absorption spectrum when the pump field is present. Using the semiconductor Bloch equations we develop a model that permits the pump-induced changes in the probe transmission to be calculated for arbitrary laser pulse profiles, both chirped and unchirped. The results demonstrate that the *amplitude* and *phase* spectral structure of the probe strongly influence the detection signal when the pulses are ultrafast (i.e., faster than the polarization decay time), in marked contrast to the normal assumptions made in transient optical spectroscopy. We examine these dynamic contributions in terms of four-wave mixing of different frequencies in the probe spectrum, and show that in addition to the optical Stark shift normally measured, there is an additional component arising from dynamic changes in the refractive index due to resonantly enhanced cross-phase modulation.

I. INTRODUCTION

Pump-probe spectroscopy is a standard technique for investigating the transient response of a medium to pulsed optical excitations. In this technique the pump pulse perturbs the absorption spectrum of the medium, which is subsequently probed after a set time delay. This method implicitly assumes that the probe pulse is too weak to induce any substantial excitation of the sample and acts only to measure the transmission at each wavelength. In this paper we shall show that this assumption is not generally valid and that the results of such an experiment can depend substantially on the internal phase and amplitude spectral structure of the probe pulse. This effect is reminiscent of the well-known "coherent artifact" produced in coherent nonlinear measurements.[1]

The optical Stark effect (OSE) in semiconductors has been the subject of considerable experimental and theoretical work in recent years.[2–8] When the pump pulse is detuned below the lowest exciton transition, the resonance frequency is increased, thus blueshifting the absorption spectrum of the exciton transition measured by the probe pulse. In addition to displaying behavior analogous to that found in atomic systems,[9] the strong coupling of excitons to phonons and carriers modifies the nonlinear optical response of semiconductors. Recent work by Lindberg and Koch[8] and Joffre *et al.*[10] has shown that new effects can arise when the pulse widths approach the phase relaxation time of the medium. In the case of excitons in GaAs quantum wells with binding energy of approximately 10 meV, this regime is experimentally accessible. The present work shows that in addition to these new temporal effects, the measured response is strongly dependent on the spectral content of the probe. We consider two regimes here, in which (i) the probe pulse (of duration T_{probe}) is faster than the exciton response (T_{ex}) and possesses a power spectrum which is not flat at the detection frequency, and (ii) the probe pulse is strongly chirped. In this way we examine the effects of both *amplitude* and *phase* structure in the probe spectrum. The experimental data are interpreted in terms of a model of the nonlinear optical response derived from the semiconductor Bloch equations.[11] The resulting expressions for the induced changes in transmission can be used with arbitrary pump and probe field distributions. Although the theory assumes Markovian damping and neglects phonon coupling between the different exciton states, these expressions provide a good qualitative account of the data and lead to the interpretation of the dynamic interaction in terms of pump-induced exciton-mediated coupling between probe frequencies inside the sample.

After presenting the details of the experiment using unchirped pulses (Sec. II), we outline the theoretical model in Sec. III. In Section IV we describe results obtained with chirped probe pulses, and demonstrate how they arise in the model. Section V describes the mechanism in terms of a mixing process. We summarize our results in Sec. VI, and present mathematical details of the model in Appendices A and B.

II. EXPERIMENTS USING BANDWIDTH-LIMITED PULSES

The transient nonlinear optical response of the heavy-hole exciton in GaAs multiple quantum wells (MQW's) was measured using time-resolved absorption spectroscopy. In this now standard technique, an intense pump pulse (here propagating along the sample growth direction) is focused through the sample and a noncollinear probe pulse is focused through the same volume (Fig. 1). The pump beam is masked off behind the sample, while the probe pulse is spectrally filtered in a

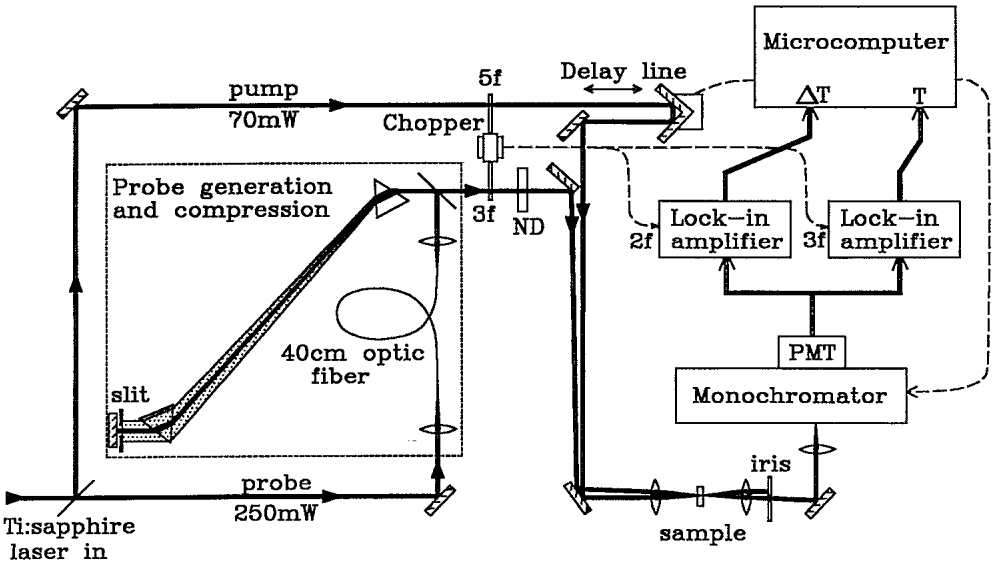

FIG. 1. Experimental arrangement used for the pump-probe experiments.

monochromator before detection by a photomultiplier. The pump-induced changes in the probe transmission are measured at set probe delay times and detection wavelengths.

The pump pulses were generated in a Ti:sapphire laser pumped by a cw multiline argon ion laser. The passive cw mode locking provided by the gain crystal (1 cm long with 0.1% doping) was stabilized using a saturable absorber jet (10^{-4} M IR140 in ethylene glycol) in a 5-cm secondary subcavity.[12] Tunable output was available between 800 and 880 nm (limited by the mirror transmission and gain bandwidth) using a 400-μm single-plate birefringent filter, with average power of 350 mW and pulse width less than 200 fs. A two-prism, negative group-velocity-dispersion (NGVD) stage inside the laser cavity was adjusted for minimum pulse width, and the output pulses were measured to be bandwidth limited.

The optical Stark effect is observed when a strong pump field, detuned below the exciton resonance (Fig. 2), is imposed on the sample. Two quantum well structures have been studied.

(i) A 76-Å GaAs/AlAs MQW sample which had an $n = 1$ heavy-hole exciton transition ($E1$-hh) at 1.488 eV at 300 K, approximately 19 meV below the $n = 1$ light-hole transition ($E1$-lh) (see Fig. 2).

(ii) A 100-Å $GaAs/Al_{0.3}Ga_{0.7}As$ MQW sample where the corresponding heavy- and light-hole exciton transition energies were 1.460 and 1.471 eV, respectively.

This large spectral separation of $E1$-hh and $E1$-lh allows us to ignore the effects of the light hole when discussing transmission changes around the heavy-hole exciton (Sec. IV A). The samples were of sufficient quality that the experiments could be performed at room temperature, and a pump detuning of 35 meV was adopted to minimize one-photon absorption while remaining near resonance. In order to produce probe frequencies around the exciton, a "continuum" was generated by focusing approximately 70% of the laser output into 40 cm of single-mode optical fiber. The combination of self-phase modulation and group-velocity dispersion considerably broadens the spectral bandwidth of the pulses (extending it to 90 meV) thus allowing measurements of the perturbed sample transmission near the exciton energy (see Fig. 2). Since the fiber-generated continuum is chirped, a NGVD stage was used to recompress the probe pulses. Average pump powers of 20 mW were used, producing peak intensities of 20 MW cm^{-2} in the sample; the probe was subsequently attenuated to a factor of 10^{-3} of the pump intensity. A phase-sensitive detection scheme was adopted to improve the signal-to-noise ratio: each beam was chopped at a different frequency before the sample, and the probe photocurrent was detected at the difference frequency. Simultaneous measurements of the abso-

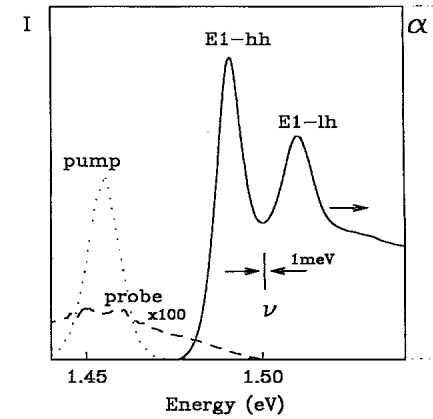

FIG. 2. Linear absorption spectrum of the 76-Å GaAs MQW sample at room temperature showing the $n = 1$ heavy-hole ($E1$-hh) and light-hole ($E1$-lh) exciton transitions. Also shown are the pump and probe spectral profiles detuned below the lowest exciton transition.

lute probe intensity allowed on-line normalization of the data in a microcomputer which also controlled a stepper-motor-driven delay line (2.5 μm or 17 fs steps) and the detection wavelength (monochromator bandpass 1 meV).

Data are presented in the conventional fashion as the differential transmission signal (DTS)

$$\mathcal{T}(\tau,\nu) \equiv \frac{I_{on}(\tau,\nu) - I_{off}(\nu)}{I_{off}(\nu)} \tag{2.1}$$

$$\simeq -\Delta\alpha(\tau)d\,, \tag{2.2}$$

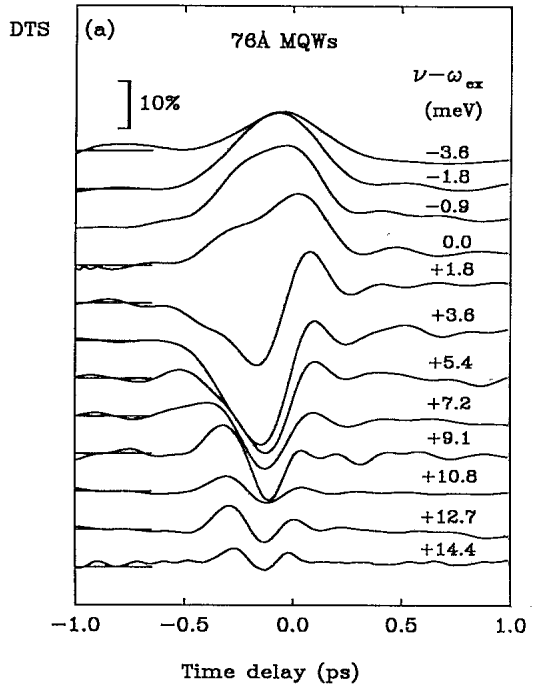

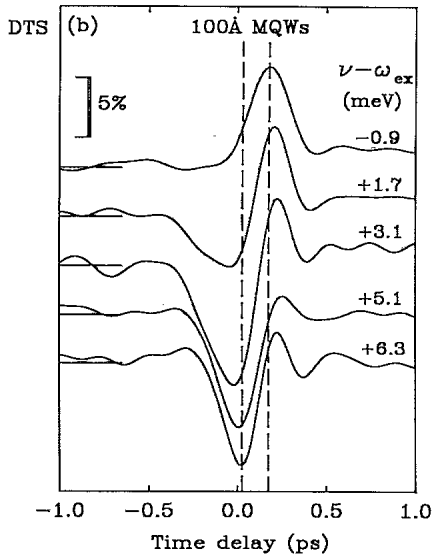

FIG. 3. The differential in transmission (DTS) measured at different values of the probe detuning Δ (meV) from the $n = 1$ heavy-hole exciton. (a) 76-Å and (b) 100-Å GaAs MQW samples at 300 K. The pump has a pulse width of 180 fs and is detuned 35 meV below the heavy-hole exciton. The unchirped probe has a bandwidth of 40 meV.

where $I_{on}(\tau,\nu)$ represents the probe intensity at the detection frequency ν when the pump pulse is also on the sample (with the peak of the pump pulse at a time τ *earlier* than the peak of the probe pulse), and I_{off} is the unperturbed transmitted probe intensity. When the change in the absorption is not too large, i.e., $\Delta\alpha d \ll 1$ where d is the sample thickness, the equality (2.2) holds, and the induced absorption coefficient $\Delta\alpha$ is directly probed. This method is conventionally used to normalize out the effects of probe intensity fluctuations and spectral structure within the continuum: it assumes a linear response of the excited medium to the probe pulse.

Figure 3 shows a series of $\mathcal{T}(\tau,\nu)$ measurements as a function of τ for different detection frequencies near the heavy-hole exciton. It can be seen that there is an ultrafast response, with an increase in *transmission* on the low-energy side of the exciton and an increase in *absorption* on the high-energy side. These features form a signature of the optical Stark effect in which the exciton absorption line is shifted to higher energy by the instantaneous pump field (a blueshift). Similar behavior is seen for both the 76- [Fig. 3(a)] and 100-Å [Fig. 3(b)] QW samples. The temporal response $\sim$250 fs is close to that of the measured cross-correlation between pump and probe beams $\tau_c = 220$ fs. The weak residual effect remaining at $\tau > \tau_c$ is tentatively ascribed to real carrier generation,[3,13] most likely by a multiphoton process, and shows the difficulty in producing a purely coherent electronic excitation of semiconductors.

In addition to these observations, which are qualitatively similar to previously reported results,[2–5] there are well-resolved details that cannot be explained in terms of an adiabatic blueshift of the exciton resonance. A difference in the time delay of the peak response is apparent either side of the exciton center [highlighted explicitly in Fig. 3(b), where it was measured to be 130 fs], and temporal scans near the exciton energy show both positive and negative DTS. Neither of these features are expected if the exciton line rigidly shifts to higher energies and returns when the pump pulse exits the sample, because this would imply that all DTS traces should be symmetrical around zero delay. To interpret these signals in terms of the pump-perturbed sample transmission at each detection wavelength requires changes in the exciton line shape.[14] The asymmetrical behavior about $\tau = 0$ implies that this evolution of line shape is not purely a function of the instantaneous pump intensity. In the theory derived in the following section we show this description to be inadequate when the optical pulse widths approach the phase scattering time of the exciton.

III. THEORY

In this section, we use the model presented by Lindberg and Koch[8,11] that derives from the semiconductor Bloch equations for electrons and holes, and extend their results to obtain more general, though computationally tractable, expressions involving arbitrary pump and probe pulse profiles. These results are later simplified by using the approximation of an isolated two-level

system to allow an analytical comparison with experiment.

A. Nonlinear response

The change in probe transmission induced by the pump pulse is calculated in Appendix A to give

$$\mathcal{T}(\nu,\tau) \simeq \frac{-\nu d}{\eta c}\mathrm{Im}\left\{\frac{P^{(3)}(\nu,\tau)}{\varepsilon_0 \mathcal{E}_p(\nu)}\right\}, \tag{3.1}$$

where $P^{(3)}(\nu,\tau)$ is the pump-induced third-order polarization of the medium, $\mathcal{E}_p(\nu)$ is the probe field, and η is the refractive index of the medium.

It is more convenient to transform into the rotating frame at the pump frequency (ω_{pump}), with respect to which all frequencies are now transformed. The pump detuning $\Omega = \omega_{\mathrm{ex}} - \omega_{\mathrm{pump}}$, where $\hbar\omega_{\mathrm{ex}}$ is the $n=1$ heavy-hole exciton transition energy, is then equal to the exciton frequency in the new rotating frame. In the present experiments, the only exciton state which needs to be included in the description is the $n=1$ heavy-hole exciton since it is spectrally well separated from all the other exciton states and in particular from the $n=1$ light-hole exciton (see Fig. 2). The expression for the induced polarization is further simplified by retaining only those terms which propagate in the original probe direction $\mathbf{k}_{\mathrm{probe}}$ (since the experiment is sensitive only to these terms), and are proportional to $\mathcal{E}_p E^* E$, where E is the pump field. The details are presented in Appendix A, and the result is

$$P^{(3)}(\nu,\tau) = \int \frac{d\delta}{2\pi}\, e^{-i\delta\tau}\, \mathcal{E}_p(\nu-\delta)\, G(\delta,\nu)\,, \tag{3.2a}$$

where the transfer function $G(\delta,\nu)$ is given by

$$G(\delta,\nu) = \left(\frac{2\mu^2\varepsilon_0}{\hbar^2}\right)\chi^{(1)}(\nu)\int \frac{d\Delta}{2\pi}\, E(\Delta)E^*(\Delta-\delta) \times D(\Delta,\delta,\nu)\,. \tag{3.2b}$$

The resonant enhancements are contained in

$$D(\Delta,\delta,\nu) = \frac{1}{\Omega+\delta-\Delta+i\gamma} \times\left[\frac{1}{\nu-\delta-\Omega+i\gamma}\frac{\nu-\Delta+2i\gamma}{\nu-\Delta+i\Gamma} + \frac{1}{\Delta-\Omega+i\gamma}\frac{\delta+2i\gamma}{\delta+i\Gamma}\right], \tag{3.2c}$$

and the linear susceptibility is

$$\chi^{(1)}(\nu) = \frac{-\mu^2/\hbar\varepsilon_0}{\nu-\omega_{\mathrm{ex}}+i\gamma}\,, \tag{3.2d}$$

μ is the oscillator strength, and γ, Γ are, respectively, the polarization and population decay rates. Assuming the exciton linewidth to be predominantly homogeneously broadened, we estimate $\gamma \simeq 5$ meV from the linear absorption spectra.

The measured signals are obtained from (3.1) and (3.2a)–(3.2d) at various time delays. These equations can be used for general pump and probe line shapes as well as for arbitrary dephasing and population decay rates. At large detuning the first term of D in (3.2c) dominates because both δ and Δ are smaller than Ω if there is to be no real absorption. An expression which bears some similarities has been derived by Burt[15] for the degenerate case where pump and probe occur both at the same frequency and time.

In Sec. V we will use (3.2a)-(3.2d) to examine the four-wave-mixing interaction. However, it is useful here to work in the large detuning approximation and, in order to produce analytical results, to further assume that only a single inelastic scattering process operates on the exciton, so that $\Gamma = 2\gamma$. Hence, from (3.2c) and (3.2d) we get

$$D(\Delta,\delta,\nu) = \left(\frac{\hbar\varepsilon_0}{\mu^2}\right)\frac{\chi^{(1)}(\nu-\delta)}{\Omega}\,, \tag{3.3}$$

which is independent of Δ. Evaluating the induced polarization using (3.2a) and (3.2b), we obtain the convenient expression

$$P^{(3)}(\nu,\tau) = \frac{2\varepsilon_0}{\hbar\Omega}\,\chi^{(1)}(\nu)\int dt\,|E(t+\tau)|^2\,\tilde{P}^{(1)}(\nu,t), \tag{3.4}$$

which represents the smearing of $\tilde{P}^{(1)}(\nu,t)$ by the finite pump pulse width. $\tilde{P}^{(1)}$ is the linear polarization in a frame rotating at the detection frequency ν:

$$\tilde{P}^{(1)}(\nu,t) \equiv e^{i\nu t}P^{(1)}(t) = e^{i\nu t}\,\varepsilon_0\int\frac{d\omega}{2\pi}\,\chi^{(1)}(\omega)\,\mathcal{E}_p(\omega)\,e^{-i\omega t}\,. \tag{3.5}$$

When the probe field enters the sample it sets up a polarization that reradiates back into the probe. The change in the probe field $\delta\mathcal{E}_p$ arises from pump-induced perturbations of this linear polarization.

The third-order polarization can be expressed in an alternative form by integrating (3.4):

$$P^{(3)}(\nu,\tau) = -\frac{2\varepsilon_0}{\hbar\Omega}\chi^{(1)}(\nu)\int dt\,A(t+\tau)\,\frac{\partial\tilde{P}^{(1)}(t)}{\partial t}\,, \tag{3.6}$$

with the time-integrated pump intensity,

$$A(t) = \int_{-\infty}^{t} dt'\,|E(t')|^2\,. \tag{3.7}$$

The rate of change of polarization obtained from (3.5) can be combined with

$$(\nu-\omega)\,\chi^{(1)}(\omega)\,\chi^{(1)}(\nu) = \frac{-\mu^2}{\hbar\varepsilon_0}\left[\chi^{(1)}(\omega)-\chi^{(1)}(\nu)\right], \tag{3.8}$$

which is valid for a Lorentzian line shape (3.2d), to give

$$P^{(3)}(\nu,\tau) = \frac{2i\mu^2}{\hbar^2\Omega}\int dt\,A(t+\tau)e^{i\nu t}\,\frac{\varepsilon_0}{2\pi}\int d\omega\,e^{-i\omega t}\mathcal{E}_p(\omega) \times\left[\chi^{(1)}(\omega)-\chi^{(1)}(\nu)\right] \tag{3.9}$$

$$= \frac{2i\mu^2}{\hbar^2\Omega}\int dt\,A(t+\tau)e^{i\nu t} \times\left[P^{(1)}(t)-\chi^{(1)}(\nu)\varepsilon_0\mathcal{E}_p(t)\right]. \tag{3.10}$$

TABLE I. The decay time of the polarization induced by the probe, $T_{\rm pol}$, is given by the convolution of the probe with pulse width $T_{\rm probe}$ and of the material response with decay time $T_{\rm ex}(\propto \gamma^{-1})$. The Stark shifts $\delta\omega_{\rm ad}$, $\delta\omega_{\rm ex}$, and the phase shift Φ are defined in (3.12), (3.16), and (3.15), respectively.

Regime	Temporal limit	Weak shift limit
Adiabatic response	$T_{\rm ex} < T_{\rm probe} < T_{\rm pump}$	$\delta\omega_{\rm ad} < \gamma$
Dynamical correction	$T_{\rm pump} < T_{\rm pol}$	$\delta\omega_{\rm ex} < \gamma$
Material-dominated dynamic response	$T_{\rm pump}, T_{\rm probe} < T_{\rm ex}$	$\Phi < \pi$
Probe-dominated dynamic response	$T_{\rm probe} < T_{\rm ex} < T_{\rm pump}$	

The two equivalent expressions (3.4) and (3.10) for arbitrary pulse profiles are useful in examining the physical processes under study. They can also be derived (in the approximation of large detuning and $\Gamma = 2\gamma$) by extending the nonlinear susceptibility formalism of Joffre *et al.*[4] To our knowledge, these results (3.4) and (3.10) have not explicitly appeared in the literature, although they may have a significant role in the interpretation of many of the pump-probe experiments performed. We shall now apply them to four different regimes, which are shown in Table I.

B. Adiabatic limit

In the adiabatic limit, we take all the field amplitudes to vary more slowly than either the polarization scattering time or the Rabi cycling time ($\sim 2\pi/\Omega$). For a probe pulse which is much shorter than the pump pulse, the third-order polarization is calculated in Appendix B to give the pump-perturbed total polarization

$$P^{\rm tot}(\nu,\tau) \equiv P^{(1)}(\nu) + P^{(3)}(\nu,\tau) = \varepsilon_0 \mathcal{E}_p(\nu) \left[\chi^{(1)}(\nu) - \delta\omega_{\rm ad}(\tau) \left.\frac{\partial\chi^{(1)}}{\partial\omega}\right|_\nu\right], \tag{3.11}$$

where

$$\hbar\delta\omega_{\rm ad}(\tau) = \frac{2|\mu E(\tau)|^2}{\hbar\Omega} \tag{3.12}$$

is the adiabatic Stark shift, $E(\tau)$ being the instantaneous pump field strength when the probe pulse arrives. Since $\delta\omega_{\rm ad}(\tau) \ll \gamma$ in the large detuning limit, we can contract the bracketed kernel of (3.11) into $\chi^{(1)}(\nu - \delta\omega_{\rm ad}(\tau))$. This is equivalent to an *increase* of the resonance energy, known as the optical Stark shift, with the absorption now centered at $\omega_{\rm ex} + \delta\omega_{\rm ad}(\tau)$. For quasi-cw intense optical fields detuned below the exciton transition, the effective absorption line seen by a weak probe beam appears to be centered around a higher energy than the unperturbed linear response. However, as the pump and probe pulses get shorter new effects appear and the spectral extents of the pump and probe start to play a role.

C. Dynamical correction to the adiabatic response

For an ultrashort pump pulse, the convolution in (3.4) can be ignored and we obtain

$$P^{(3)}(\nu,\tau) = -\frac{2\varepsilon_0}{\hbar\Omega} A(\infty)\, \chi^{(1)}(\nu)\, \tilde{P}^{(1)}(\nu,-\tau)\,. \tag{3.13}$$

Thus the time-resolved nonlinear signal follows the linear polarization induced by the probe pulse. The sign of τ follows from the conventional definition of time delay and is reversed in comparison to time-resolved experiments involving incoherent nonlinearities.[16] In the latter case the above band-gap pump pulse deposits energy into the medium, which relaxes back to the ground state over a longer time. The probe then measures how quickly this decay occurs by measuring the excited-state energy distribution in the medium. In the present coherent regime, it is the probe which "deposits" a polarization in the medium, and this subsequently relaxes over time. The pump in effect "probes" this decay by perturbing the polarization, although no pump energy is absorbed and the signal is detected on the probe beam.

Again, using the Lorentzian line shape (3.2d), and (B3) with (3.13), the change in the total polarization can be written as

$$P^{\rm tot}(\nu,\tau) = \varepsilon_0 \mathcal{E}_p(\nu)\chi^{(1)}(\nu) - \frac{\Phi}{\chi^{(1)}(\nu)} \left.\frac{\partial\chi^{(1)}}{\partial\omega}\right|_\nu \tilde{P}^{(1)}(\nu,-\tau)\,, \tag{3.14}$$

where

$$\Phi = \frac{2\mu^2 A(\infty)}{\hbar^2\Omega} = \int dt\, \delta\omega_{\rm ad}(t) \tag{3.15}$$

is the integrated phase shift produced by the pump. Hence, similarly to (3.11) we obtain a frequency shift of the exciton

$$\delta\omega_{\rm ex}(\tau) = \Phi \times \frac{\tilde{P}^{(1)}(\nu,-\tau)}{P^{(1)}(\nu)}\,, \tag{3.16}$$

providing $\delta\omega_{\rm ex}(\tau) \ll \gamma$. The final factor, which is independent of the oscillator strength, contains the correction to the adiabatic regime from the dynamic response and, as it is complex, can represent changes in both energy and line shape of the excitonic response.

D. Material-dominated dynamic response

In order to recover the regime considered by Joffre *et al.*,[4] we assume that both pump and probe pulse widths are considerably shorter than the polarization decay time, so that $E(t) = E_0\,\delta(t)$. Using (3.10) we obtain

$$P^{(3)}(\nu,\tau) = i\Phi \int dt\, \theta(t+\tau)\, e^{i\nu t} \times \left[P^{(1)}(t) - \chi^{(1)}(\nu)\varepsilon_0 \mathcal{E}_p(t)\right], \quad (3.17)$$

where Φ is defined in (3.15). For $\tau < 0$ (when the pump pulse arrives after the probe) $\theta(t+\tau)\mathcal{E}_p(t) = 0$ for all t, since the the probe pulse is short. Thus we can drop the final term in (3.17), and, after an inverse Fourier transform, we get the total perturbed polarization in the rotating frame at the detection frequency (cf. 3.5)

$$\tilde{P}^{\text{tot}}(t,\tau) \equiv e^{i\nu t} \int d\omega\, e^{-i\omega t}\, P^{\text{tot}}(\omega,\tau) \simeq \begin{cases} \tilde{P}^{(1)}(t)\, e^{i\Phi} & t > -\tau \\ \tilde{P}^{(1)}(t) & t < -\tau, \end{cases} \quad (3.18)$$

which shows that the effect of the pump is to induce an extra phase shift on the probe polarization. The size of this phase shift is determined by the integrated intensity of the pump pulse. This "jarring" of the polarization introduces a phase discontinuity of the radiating polarization, whose effects persist for all times after the arrival of the pump pulse. This leads to the "reversed" dynamics observed experimentally.[4,5]

E. Probe-dominated dynamic regime

Having examined some of the implications for the optical nonlinearity within a short pulse approximation, we now examine the conditions pertaining to our experiments presented in Sec. II, namely, when the probe pulse width is shorter than the material response time which in turn is shorter than the pump pulse width (T_{pump}). The results obtained depend on the fact that the unchirped probe pulse does not have a symmetrical spectrum around the exciton resonance, and that the probe bandwidth is large compared to γ.

The spectral asymmetry of the probe is assumed to be weak around the observation frequency so we can write $\mathcal{E}_p(\nu-\omega) = \mathcal{E}_p(\nu) - \omega\partial\mathcal{E}_p/\partial\nu$. Using this in (3.9) together with the time-integrated pump pulse intensity (3.7) yields

$$P^{(3)}(\nu,\tau) \propto \int dt\, e^{i\nu t}\chi^{(1)}(t) \left\{\mathcal{E}_p(\nu)\left[A(t+\tau) - A(\tau)\right] - \frac{\partial\mathcal{E}_p}{\partial\nu}\left[|E(t+\tau)|^2 - |E(\tau)|^2\right]\right\}, \quad (3.19)$$

where $\chi^{(1)}(t)$ has an exponential decay for $t > 0$. When this decay is fast compared to the pump pulse ($\gamma T_{\text{pump}} > 1$), we need retain only the first-order terms in the Taylor expansions of $|E(t+\tau)|^2$ and $A(t+\tau)$ [defined in (3.7)] for small t, hence

$$P^{(3)}(\nu,\tau) \propto \frac{\partial\chi^{(1)}}{\partial\nu} \left\{\mathcal{E}_p(\nu)\,|E(\tau)|^2 - \frac{\partial\mathcal{E}_p}{\partial\nu}\,\frac{\partial|E|^2}{\partial t}\bigg|_\tau\right\}. \quad (3.20)$$

When there is no spectral asymmetry in the probe ($\frac{\partial\mathcal{E}_p}{\partial\nu} = 0$), (3.20) yields a signal whose amplitude follows the pump pulse profile as expected of an adiabatic Stark shift. When the probe spectrum has a spectral asymmetry at the observation frequency ($\frac{\partial\mathcal{E}_p}{\partial\nu} < 0$), the second term in 3.20 can be negative for times after the peak of the pump pulse ($\tau > 0$) so that $P^{(3)}(\nu,\tau)$ can change sign at $\tau = 0$. For this to happen, the asymmetry in the probe spectrum must be such that

$$\frac{\nu - \omega_{\text{probe}}}{\Delta\omega^2_{\text{probe}}}\,\frac{2\tau}{T^2_{\text{pump}}} > \frac{1}{(4\ln 2)^2}, \quad (3.21)$$

where bandwidth-limited Gaussian pulses have been assumed. This result shows that two conditions must be satisfied for the observation of the asymmetrical temporal response. First, the pump pulse should be short, and second, the probe center frequency (ω_{probe}) should be detuned from the exciton center (about one bandwidth here). These conditions correspond to both spectral *and* dynamical conditions on the experimental parameters. For the experiments described in Sec. II, the inequality (3.21) is easily satisfied for time delays shorter than the pump pulse width.

With the above conditions in mind, (3.4) has been used to compute the response for unchirped pump and probe pulses of different bandwidths but centered at the same frequency, 35 meV below the heavy-hole exciton (Fig. 2). The calculations (Fig. 4) show qualitative agreement with the experimental data of Fig. 3, displaying the same evolution from induced absorption to transmission as the probe center frequency is tuned through the exciton resonance. Clearly visible, especially for small detunings, are temporal responses that change sign around zero de-

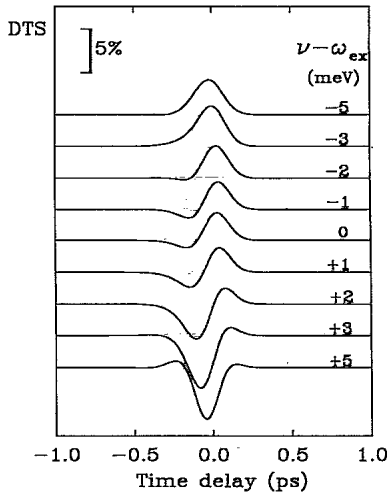

FIG. 4. DTS computed from the model (3.2a)–(3.2d) for unchirped pulses at different detection energies Δ, around the heavy-hole exciton. The parameters used were $T_{\text{pump}} = 180$ fs, $\gamma = 5$ meV, and $\Delta\omega_{\text{probe}} = 40$ meV.

lay, in excellent agreement with the experimental results.

It should be emphasized that although the probe pulse is sufficiently weak to induce only a linear response, the amplitude structure of the probe spectrum still affects the observed pump-induced transmission changes. This contrasts with the normal assumption that each probe frequency simply examines the sample absorption at that frequency. In Sec. V we will examine this result from the point of view of a nonlinear mixing between the different frequencies in the probe.

IV. EXPERIMENTS USING CHIRPED PULSES

Having examined the implications of *amplitude* structure on the probe pulse we now turn our attention to the effects of *phase* structure within its spectrum. Recent interest in chirped pulses has focused on whether they can provide new information about the polarization decay of two-level systems.[17,18] In experiments using semiconductor-doped glass samples for example, the introduction of chirp had little effect on the observed decay[17] even though the pulses were stretched by a factor of 50. However, recent measurements of solutions of the dye resorufin have shown that chirped pulses can isolate non-Markovian contributions to the phase scattering.[18] Here, we shall examine the influence of a chirped probe on the OSE in a semiconductor.

A. Chirped probe: experimental results

In the experiments conducted here, the nonlinear interaction is proportional to $\mathcal{E}_p E E^*$ so that the pump enters only through its intensity, and changing its frequency has little effect for large detuning. We thus concentrate on experiments that use a chirped probe pulse,

$$\mathcal{E}_p(t) = \mathcal{E}_p^0 \exp\left\{-at^2 - i\phi_p(t)\right\}, \tag{4.1}$$

where

$$\phi_p(t) = (\omega_{\text{probe}} + bt)t, \tag{4.2}$$

and $a = 2\ln 2/T^2_{\text{probe}}$. We take the chirp parameter $b > T^{-2}_{\text{probe}}$, so that the probe pulse is in the strongly chirped regime, i.e., the chirp produces the dominant contribution to the probe bandwidth (the condition $b = T^{-2}_{\text{probe}}$ corresponds to the limit where the bandwidth product becomes a factor of $\sqrt{2}$ larger than its minimum value). To achieve this the pulse is passed through a longer length ($\sim$ 1 m) of optical fiber in the continuum generation stage. The resultant chirp is measured by cross-correlation with the pump pulse, and extends to 800 fs for the same probe bandwidth as before, thus satisfying the strong chirp condition.

Data obtained from the 76-Å sample (again at room temperature) are shown in Fig. 5 at detection wavelengths around the heavy-hole exciton transition. New oscillations are evident at time delays for which both pulses are present in the sample. A more complete set of data is shown in Fig. 6 for the 100-Å sample at 150 K. It can be seen that the features found in the previous

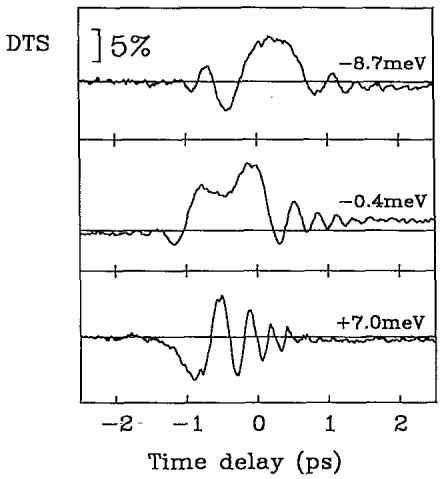

FIG. 5. Differential transmission measurements in the region of the exciton energy obtained using a strongly chirped probe pulse ($b = 6$ meV ps^{-1}) from the 76-Å GaAs MQW sample at 300 K. The width of the temporal cross-correlation is 800 fs.

experiments with an unchirped probe are still present—namely, an increase (decrease) in transmission on the low- (high-) energy side of the exciton transition. Superimposed on these features are oscillatory components with an amplitude similar to that previously obtained in the Stark response, suggesting that their origins could be related. The oscillations are most apparent at times after the pump pulse has arrived and resemble the decaying amplitude of an impulsively driven oscillator. The temporal shift in the position of the oscillatory components with detuning is the same as that expected from the different arrival time of each instantaneous frequency (ω_{inst}) at the sample. Since $\omega_{\text{inst}} \equiv \frac{\partial\phi_p(t)}{\partial t}$, this arrival time is given by $2b\tau = (\omega_{\text{inst}} - \omega_{\text{probe}})\tau$. The value of b which fits the observed temporal shift, $b = 6$ meV ps^{-1}, matches well with the value measured by cross-correlation with the pump pulse.

Also present in Fig. 6, at early times ($\tau \sim -1$ ps) near $\Delta = 10$ meV, are features deriving from the optical Stark shift of the light-hole exciton. The amplitude of this response is suppressed by a factor of approximately 4 due to the different pump detuning and polarization selection rules.[19] Because the response is weak and localized near the light-hole exciton transition we are justified in ignoring its contribution at the heavy-hole exciton transition in the following analysis.

B. Simple model

The model developed in Sec. III is used here to analyze the effect of a chirped probe pulse. Initially we assume that the phase scattering time is much faster than the optical pulse widths, and that the slower probe pulse controls the time scale of the linear polarization. Then (3.5) becomes

$$\tilde{P}^{(1)}(\nu, -\tau) = \varepsilon_0 \chi^{(1)}(\nu)\, \tilde{\mathcal{E}}_p(-\tau), \tag{4.3}$$

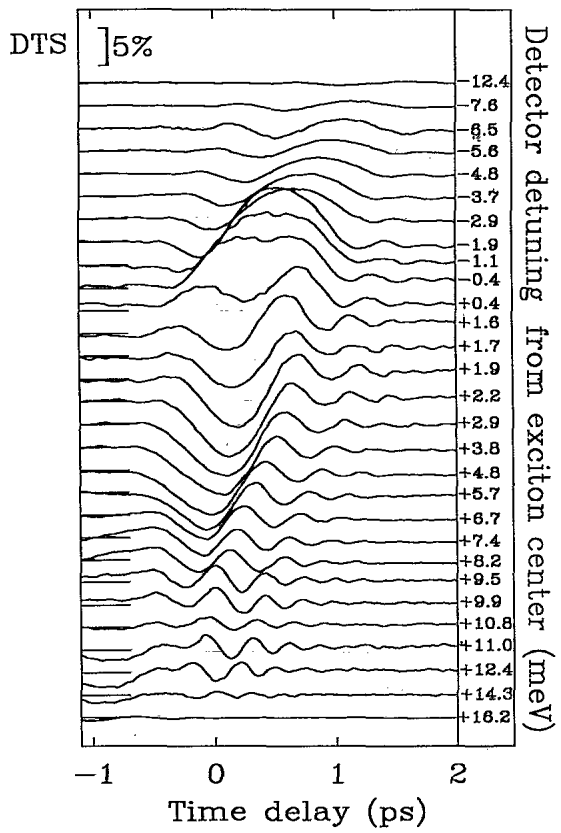

FIG. 6. DTS measurements for the 100-Å GaAs MQW sample at 150 K using a chirped probe (as in Fig. 5). In addition to the heavy-hole response, the signals around $\Delta \simeq +10$ meV and $\tau \simeq -1$ ps arise from the Stark shift of the light-hole exciton.

where the probe field in the frame rotating at the detection frequency is given by $\tilde{\mathcal{E}}_p(-\tau) = e^{-i\nu\tau}\mathcal{E}_p(-\tau)$. Using (3.14)

$$P^{(3)}(\nu,\tau) = -\Phi \left.\frac{\partial\chi^{(1)}}{\partial\omega}\right|_{\nu} \tilde{\mathcal{E}}_p(-\tau)\,. \tag{4.4}$$

From (3.1), $\mathcal{T} \propto \mathrm{Im}\{P^{(3)}\}$, thus one quadrature of the probe field (in the rotating frame) is measured directly. It is now convenient to redefine the time delay relative to the arrival time of the probe frequency centered at the exciton resonance (ω_{ex}) rather than the pulse center frequency (ω_{probe}). Using (3.1), (4.1), and (4.4) yields the DTS

$$\mathcal{T}(\tau,\nu) \propto e^{-a\tau^2}\cos\{[(\omega_{\mathrm{ex}}-\nu)-b\tau]\tau+\psi\}\,, \tag{4.5}$$

where the function ψ is independent of τ but depends on the detection detuning $\omega_{\mathrm{ex}} - \omega_{\mathrm{probe}}$. This expression shows that there are oscillations in the DTS as a function of τ, arising from the chirped probe field expressed in the rotating frame of the detection frequency. For detection at the exciton line center ($\nu = \omega_{\mathrm{ex}}$) (4.5) predicts oscillations of increasing frequency with increasing time delay. The number of fringes, n, visible under the DTS temporal envelope [within the full width at half maximum (FWHM)] can be estimated by $n \simeq bT^2_{\mathrm{probe}}/2\pi$. For the parameters used here, $n \simeq 1$, in agreement with the experimental data (Fig. 5). However, (4.5) predicts that the fringes should be symmetrical around zero delay since $\mathcal{T} \propto \cos(b\tau^2+\psi)$; this is clearly *not* seen in the experiment. Thus a more complete analysis is required to take into account the material response time. This requires a numerical solution of the response function.

C. Comparison with theory

Combining the expression (3.2a) with the optical fields and the material response described by $\Gamma = 3$ meV and $\gamma = 5$ meV, the theoretical differential transmission spectra have been computed as a function of time delay and detection energy and the result is presented in Fig. 7. Qualitatively the model reproduces the experimental results extremely well, with the oscillations partially mapping out one quadrature of the probe field (in the rotating frame at the detection frequency). Oscillations on the trailing edge are clearly displayed, with the temporal shifts of the oscillatory features again following those of the instantaneous probe frequency. By varying the parameters, we could identify three processes which might be responsible for the temporal asymmetry in the DTS scans described above.

(i) The first of these arises because of the comparable time scales of the pulse widths and the polarization scattering. As discussed by Joffre *et al.*,[10] the effect of this condition is to produce the peak response at times *preceding* zero delay. This occurs because the signal arises

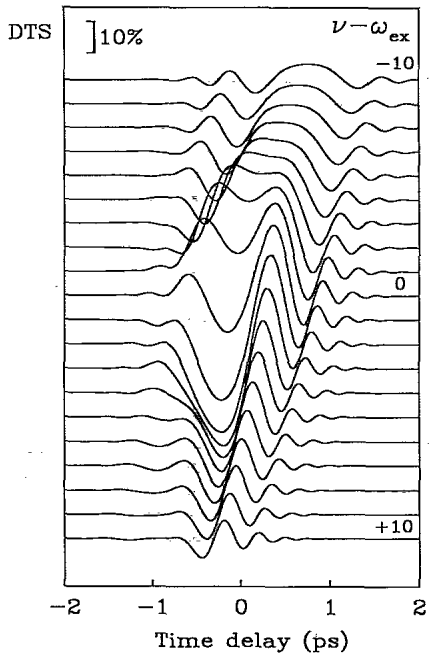

FIG. 7. Computed DTS obtained from (3.2a)–(3.2d), for different values of the probe detuning around the heavy-hole exciton (the traces are at 1-meV intervals). The probe pulse is heavily chirped. The parameters used were $T_{\mathrm{pump}} = 180$ fs, $\gamma = 5$ meV, $\Gamma = 3$ meV, and $\Delta\omega_{\mathrm{probe}} = 35$ meV.

from the perturbation of the probe polarization by the pump pulse, and this polarization is only half its maximum value at zero delay. Such a signal envelope is in contradiction to that measured experimentally in which the peaks on the trailing edge are stronger than those on the leading edge (Fig. 5).

(ii) The second process has already been discussed in Sec. III E. As the continuum becomes more spectrally structured around the exciton line, the contribution of the signals at early time delay can be suppressed while those at later times are enhanced, so that oscillations on the trailing edge become as large as the main signal. While this mechanism agrees qualitatively with the observed modulation of the DTS envelope, we find that it overestimates the magnitude of the effect.

(iii) The third contribution arises from the balance between population (Γ) and polarization (γ) scattering rates. The population scattering rate here refers to inelastic scattering of excitons (spectral diffusion rather than recombination) while the phase scattering can be somewhat larger than half this rate.[20] In this case a redistribution of signal is obtained, which is similar to that arising from amplitude structure in the probe spectrum.

In the present experiment, the effect of the first process (i) is negligible, while both (ii) and (iii) are needed to give a satisfactory fit to the results. The discrepancies with the data lie mainly in the overestimate of the amplitude of the oscillations on the trailing edge relative to the height of the central peak (see Figs. 5–7).

This analysis is, however, incomplete, since at least two potentially important effects have not been included in the model, namely, the effect of a real carrier population and the influence of non-Markovian processes in the excitation decay. As seen from the experimental data in Fig. 5, there is a longer-term residual decay of the induced transmission, probably due to real carriers created by the pump pulse. Recent theoretical work by Kuznetsov[21] shows that, when the decay times of the carrier population and the polarization are of the same order of magnitude, both have to be taken into account simultaneously in the equations. This suggest that the real carriers created by the pump may exert an influence on the polarization responsible for the OSE. Moreover, due to the time-energy uncertainty principle, carriers created by the short pump pulse are distributed over a broad region of k space. The k dependence of the form factor for the exciton-phonon interaction then leads to k dependent damping coefficients and non-Markovian behavior is expected. However, neither the exact results obtained by Kuznetsov[22] nor a Gauss-Markov model of non-Markovian damping[18] are tractable enough to permit detailed comparison with our experiment. In any event, the experimental data are already complicated by probe spectral asymmetries and real carrier effects so that such detailed comparison is currently unwarranted.

V. DEPENDENCE ON BANDWIDTH

In the preceding section we showed that the DTS depends markedly on the amplitude and phase structure of the probe pulses. Another way to examine this effect is from the point of view of a four-wave-mixing process. The mediation of the exciton in the nonlinear response to the pump pulse allows the transfer of energy between different frequencies in the probe continuum. Equations (3.2a)–(3.2d) show that the nonlinearity introduces a coupling between the detection channel ν, and other frequency components of the continuum. Thus the light emerging at the detection frequency can depend on the probe light entering the sample at *other* frequencies, i.e., on the structure of the continuum.

The transfer function $G(\delta,\nu)$ that modulates the process is determined by the interaction of the pump pulse and the sample. It is enhanced for detection channels ν near the exciton energy. Its bandwidth δ is jointly controlled by the pump bandwidth and the exciton linewidth so that ultrashort pump pulses and fast polarization scattering rates increase the bandwidth of frequencies in the probe spectrum that couple together. It occurs in the dynamic regime due to the presence of a large range of photon energies within the pump pulse which allows for a correspondingly wide redistribution of probe photon energies via the four-photon interaction.

The time-delay dependence of the response is given by the Fourier transform (with respect to the frequency separation δ) of $\mathcal{E}_p(\nu-\delta)G(\delta,\nu)$. For small probe bandwidths the coupling is restricted in range and the Fourier transform follows the slow temporal behavior of the probe pulse. The change in the transmitted probe is then determined by the imaginary part of the transfer function, $\mathrm{Im}\{G(\delta=0,\nu)\}$. This reproduces the adiabatic Stark response as the probe pulse is now long, and averages over the faster details of the response. A similar result obtains if the time-delay-integrated response is computed from the DTS using (3.1) and (3.2a) since

$$\langle \mathcal{T}(\nu)\rangle \equiv \int d\tau\, \mathcal{T}(\nu,\tau) \propto \mathrm{Im}\{\mathcal{E}_p(\nu)G(0,\nu)\} . \tag{5.1}$$

As the probe bandwidth is increased, more widely separated frequencies can couple energy into and out of the detection channel. We now consider this mixing for detection frequencies just above the exciton resonance, with unchirped probe pulses shorter than the pump pulse (i.e., the same parameters as used in Fig. 4). The intensity transfer from $\mathcal{E}_p(\nu+\delta)$ into the detection channel is proportional to $\mathrm{Im}\{e^{i\delta\tau}G(-\delta,\nu)\}$ which is shown in Fig. 8 on the rising and trailing edges of the pump pulse. This shows that at times on the rising edge of the pump pulse ($\tau<0$), energy is transferred from higher to lower energies. The direction of transfer reverses on the trailing edge of the pump pulse. This mechanism is closely related to cross-phase modulation (XPM) and we term it resonantly enhanced XPM. The refractive index experienced by the probe is enhanced as the leading edge of the pump pulse Stark shifts the exciton to higher energies. This generates a refractive index gradient ($\frac{\partial\eta}{\partial t}$) across the probe pulse bandwidth which further separates the phase fronts of the probe, generating lower frequency light. At time delays $\tau>0$, the probe "sees" the trailing edge of the pump pulse and the refractive index decreases as the exciton resonance returns to its unperturbed energy.

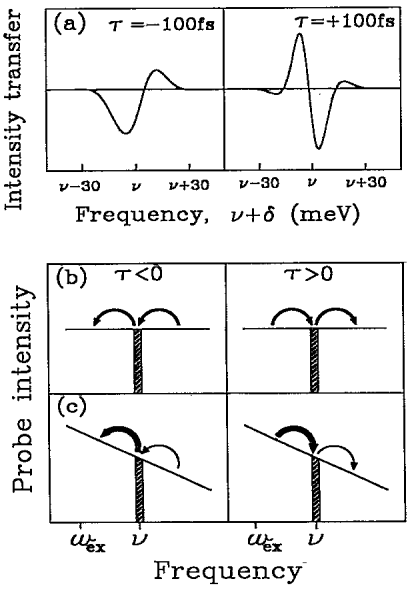

FIG. 8. (a) The intensity contributed to the detection frequency $\nu = \omega_{ex} + 2$ meV from surrounding probe frequencies at $\nu + \delta$. This coupling arises from the expression $-\mathrm{Im}\{e^{i\delta\tau}G(-\delta,\nu)\}$ as a function of separation from the detection frequency and is shown at time delays on the leading ($\tau < 0$) and trailing ($\tau > 0$) edges of the pump pulse. The direction of frequency transfer reverses either side of zero delay. (b) The intensity transfer inside a spectrally flat, unchirped probe continuum showing the redshift at early times and the blueshift at late times when the detection frequency is just above the exciton energy. (c) The intensity transfer when the probe continuum is structured which shows the origin of the extra contribution to the probe transmission: more light is coupled out at early times and in at late times.

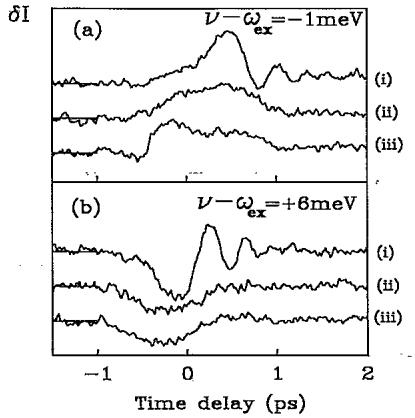

FIG. 9. Pump-induced changes in the detected probe intensity for different probe bandwidths at the sample. In the upper traces (i) frequencies at ν and below were allowed to impinge upon the sample, whereas in the lower traces (iii) the probe is composed of ν and above. The central traces (ii) are using a narrow bandwidth around ν.

This correspondingly blueshifts the probe. If we now examine detection channels below the exciton transition energy the situation is reversed because the refractive index decreases when the pump field is applied, and so the probe is blueshifted at $\tau < 0$ and redshifted at $\tau > 0$.

Using these ideas, an alternative explanation can be developed for the experiments with unchirped pulses which detect both positive and negative DTS at the same detection frequency ($\nu \sim 2$ meV in Fig. 3). If the probe spectrum is symmetrical around ν, then the energy transferred into the detection channel by XPM-assisted coupling is balanced by that transferred out [Fig. 8(b)] so that only the OSE response is detected. For an asymmetrical probe spectrum, the energy transferred into the detection frequency by the leading edge of the pump pulse is less than that coupled out, so the DTS aquires an extra negative contribution [Fig. 8(c)]. On the trailing edge of the pump pulse, more energy is coupled in than out and thus a positive contribution results. If the asymmetry is large enough, these XPM-assisted components can mask the adiabatic response, leaving the temporal scans as shown (Fig. 4). The response measured in this arrangement is thus a superposition of the OSE (the quasistatic absorptive shift) and resonantly enhanced XPM (the dynamic refractive-index shift), and it is the latter which is so sensitive to the spectral structure of the probe.

If probe intensity is only present on one side of the detection channel, the energy flows can be upset and result in the production of light beyond the existing bandwidth of the probe spectrum. This significantly upsets the experimental analysis since instead of measuring the transmission characteristics of a preexisting probe wavelength, we now detect the *generation* of light at this wavelength, even if none was there prior to it reaching the sample. We have seen evidence for this when the high-energy tail of the continuum was arranged to fall near the exciton energy. Such scans show detectable amounts of light emerging from the sample at wavelengths where effectively none enters.

It is instructive to examine the energy transfer in the case of a chirped probe pulse since then the different frequencies which couple into the detection channel arrive at different time delays, thus unfolding the unchirped DTS reponse. Figure 9 shows experimental data, in which the probe spectrum was filtered using a slit in the Fourier plane to mask off the continuum on either side of the detection frequency ν. Just below the exciton energy (a), it can be seen that both lower (i) and higher (iii) probe frequencies couple into the detection bandwidth. The central trace (ii) shows the return to the adiabatic Stark shift when only a narrow probe bandwidth (3 meV) around ν is allowed to impinge on the sample. Above the exciton energy (b), however, there is insufficient light at higher probe frequencies (iii) to contribute to the DTS although the lower frequencies (i) still generate the characteristic oscillatory components.

VI. CONCLUSION

The nonlinear optical response of semiconductors measured in these experiments includes a complicated mi-

gration of energy within the spectral bandwidth of the probe. This is in contrast to the comparable self-phase-modulation process in optical fibers and is due to the near-resonant contribution from the exciton. We have shown that both amplitude and phase structure in the probe spectrum can substantially alter the interpretation of ultrafast pump-induced changes in probe transmission. The model which we have presented explains the observations well and provides theoretical results that can be used in the interpretation of ultrafast differential transmission signals. It facilitates several equivalent descriptions of the effects by examining the mechanism from both temporal and spectral viewpoints. In particular this highlights the joint role of cross-phase-modulation and absorption line shifts in the ultrafast pulse domain. Time-resolved four-wave-mixing experiments allow the identification of the XPM process in addition to the conventionally assigned OSE absorption changes. The sensitivity to the phase as well as the amplitude of the polarization may help in the identification of non-Markovian components in the phase scattering processes. In particular the use of chirped pulses is advantageous when the probe pulse is spectrally analyzed because the XPM component then extracted is very sensitive to details of the four-wave-mixing interaction.

ACKNOWLEDGMENTS

The authors gratefully acknowledge the support of the SERC and J.J.B. thanks Jesus College, Oxford for financial provision. We would also like to thank Steve Barnett for fruitful discussions.

APPENDIX A: DERIVATION OF DTS

Using the definition of the DTS in (2.1), we write

$$\mathcal{T}(\nu,\tau) \equiv \frac{|\mathcal{E}_p(\nu)+\delta\mathcal{E}_p(\nu,\tau)|^2 - |\mathcal{E}_p(\nu)|^2}{|\mathcal{E}_p(\nu)|^2} \simeq 2\,\mathrm{Re}\left\{\frac{\delta\mathcal{E}_p(\nu,\tau)}{\mathcal{E}_p(\nu)}\right\} . \tag{A1}$$

Lindberg and Koch[8] show that in the slowly-varying-amplitude approximation, and for a short length of medium d with refractive index η, the contribution to the probe field at frequency ν arising from the pump-perturbed polarization is

$$\delta\mathcal{E}_p(\nu,\tau) = \frac{i\nu d}{2\varepsilon_0\eta c}\,P^{(3)}(\nu,\tau) . \tag{A2}$$

Substituting (A2) into (A1) gives the expression (3.1). The nonlinear polarization induced by the pump has been calculated in Ref. 8 to give

$$P^{(3)}(\nu,\tau) = \varepsilon_0 \int_{-\infty}^{\infty} dt\, e^{i\nu t} \int_{-\infty}^{t} dt' \mathcal{E}_p(t')\delta\chi(t,t',\tau) , \tag{A3}$$

where $\delta\chi(t,t',\tau)$ is the third-order change in susceptibility given by[8]

$$\begin{aligned}\delta\chi(t',t) = {} & e^{-(i\Omega+\gamma)(t-t')}\left\{\int_0^\infty dt_2\, E(t'-t_2)\, e^{-\Gamma t_2}\int_0^\infty dt_3\, E^*(t'-t_2-t_3)\, e^{(i\Omega-\gamma)t_3} + \text{c.c.}\right\} \\ & + e^{-\Gamma(t-t')}\int_0^{t-t'} dt_2\, E(t-t_2)\, e^{-(i\Omega+\gamma-\Gamma)t_2}\int_0^\infty dt_3\, E^*(t'-t_3)\, e^{(i\Omega-\gamma)t_3} \\ & + e^{-(i\Omega+\gamma)(t-t')}\int_0^{t-t'} dt_2\, E(t-t_2)\int_0^{t-t'-t_2} dt_3\, E^*(t-t_2-t_3)\, e^{(i\Omega+\gamma-\Gamma)t_3} .\end{aligned} \tag{A4}$$

Lindberg and Koch go on to choose simplified expressions for trial pulses that do not include those of interest here. It is, however, possible to develop a reasonably simple and tractable expression that both yields to computational evaluation and conveys some insight into the physics.

It is best to reform the expression so that the optical fields are evaluated at the same time points, by interchanging the t and t' integrals and substituting new t_2 and t_3 variables into the last two terms. Combining this with (A2) results in

$$\begin{aligned}\delta\mathcal{E}_p(\nu) = {} & \int dt' \int dt\ \ \theta(t)\,\mathcal{E}_p(t')\, e^{i(\nu-\Omega+i\gamma)t}\, e^{i\nu t'} \\ & \times\left\{\begin{array}{lll} \displaystyle\int_0^\infty dt_2\, e^{-\Gamma t_2} & \displaystyle\int_0^\infty dt_3\, e^{(i\Omega-\gamma)t_3} & E(t'-t_2)E^*(t'-t_2-t_3) + \text{c.c.} \\ \displaystyle+\int_{-t}^0 dt_2\, e^{(\Gamma-2\gamma)t_2} & \displaystyle\int_{-t_2}^\infty dt_3\, e^{(i\Omega-\gamma)t_3} & E(t'-t_2)E^*(t'-t_2-t_3) \\ \displaystyle+\int_{-t}^0 dt_2 & \displaystyle\int_0^{-t_2} dt_3\, e^{(i\Omega+\gamma-\Gamma)t_3} & E(t'-t_2)E^*(t'-t_2-t_3)\end{array}\right\} .\end{aligned} \tag{A5}$$

Further progress is made by Fourier transforming the pump fields to get

$$E(t'-t_2)E^*(t'-t_2-t_3)=\iint \frac{d\Delta}{2\pi}\frac{d\delta}{2\pi}\; E(\Delta)E^*(\Delta-\delta)\,e^{i(\delta-\Delta)t_3+i\delta t_2-i\delta t'}\,. \tag{A6}$$

It is now possible to evaluate the integral in t' producing $\mathcal{E}_p(\nu-\delta)$. By reversing the sign of t_2, and the order of integration in the final term in (A5), it is also possible to evaluate the integral in t, using the relation

$$\int dt'\,\theta(t'-t)\,e^{i\zeta t'}=\frac{i}{\zeta}\,e^{i\zeta t}\,. \tag{A7}$$

This results in the simplified expression

$$\delta\mathcal{E}_p(\nu)=i\int\frac{d\Delta}{2\pi}\int\frac{d\delta}{2\pi}\,\mathcal{E}_p(\nu-\delta)E(\Delta)E^*(\Delta-\delta)\frac{D(\Delta,\delta,\nu)}{\nu-\Omega+i\gamma}\,, \tag{A8}$$

where

$$\begin{aligned}D(\Delta,\delta,\nu)=&\int_0^\infty dt_2\,e^{i(\delta+i\Gamma)t_2}\int_0^\infty dt_3\,e^{i(\Omega+\delta-\Delta+i\gamma)t_3}\;+\;\text{c.c.}\\&+\int_0^\infty dt_2\,e^{i(\nu-\Omega-\delta+i\Gamma-i\gamma)t_2}\int_{t_2}^\infty dt_3\,e^{i(\Omega+\delta-\Delta+i\gamma)t_3}\\&+\int_0^\infty dt_3\;\;e^{i(\Omega+\delta-\Delta+i\Gamma-i\gamma)t_3}\;\;\int_{t_3}^\infty dt_2\,e^{i(\nu-\Omega-\delta+i\gamma)t_2}\,.\end{aligned} \tag{A9}$$

When the integrals in t_2 and t_3 are evaluated using (A7) the simple expression for the propagator D, given in (3.2c), is obtained. To make the resulting expressions more transparent it is useful to give the two pulses their own time origin, so that their Fourier transforms do not contain high frequencies arising from a time shift. We set the pump to arrive at $t=-\tau$, and the probe at $t=0$, and factor out the time shift of the pump arrival time. The result is given in Eqs. (3.2a)–(3.2d).

APPENDIX B: DERIVATION OF ADIABATIC LIMIT

In the adiabatic regime, the spectral width of the probe is narrower than the exciton linewidth. Hence (3.5) becomes

$$\tilde{P}^{(1)}(\nu,t)=e^{i\nu t}\varepsilon_0\chi^{(1)}(\nu)\mathcal{E}_p(t)\,. \tag{B1}$$

We also work in the limit in which the probe pulse is shorter than the pump pulse so that it probes the system at one particular value of the pump intensity. Thus substituting (B1) into (3.4) projects out the pump field at $t=\tau$, leaving

$$P^{(3)}(\nu,\tau)=\frac{2|E(\tau)|^2}{\hbar\Omega}e^{i\nu t}\left[\varepsilon_0\chi^{(1)}(\nu)\right]^2\mathcal{E}_p(\nu)\,. \tag{B2}$$

Using the Lorentzian line shape (3.2d), and taking $\omega\to\nu$ in (3.8), we get

$$\left[\chi^{(1)}(\nu)\right]^2=\frac{\mu^2}{\hbar\varepsilon_0}\left.\frac{\partial\chi^{(1)}}{\partial\omega}\right|_\nu\,. \tag{B3}$$

The expression (3.14) then results straightforwardly from (B2) and (B3).

[1] C.V. Shank and D.H. Auston, Phys. Rev. Lett. **34**, 479 (1975).
[2] A. Mysyrowicz, D. Hulin, A. Antonetti, A. Migus, W.T. Masselink, and H. Morkoç, Phys. Rev. Lett. **25**, 2748 (1986).
[3] A. Von Lehmen, D.S. Chemla, J.E. Zucker, and J.P. Heritage, Opt. Lett. **11**, 609 (1986).
[4] M. Joffre, D. Hulin, A. Migus, and A. Antonetti, J. Mod. Opt. **35**, 1951 (1988).
[5] N. Peyghambarian, S.W. Koch, M. Lindberg, B. Fleugel, and M. Joffre, Phys. Rev. Lett. **62**, 1185 (1989).
[6] S. Schmitt-Rink and D.S. Chemla, Phys. Rev. Lett. **57**, 2752 (1986).
[7] S. Schmitt-Rink, D.S. Chemla, and H. Haug, Phys. Rev. B **37**, 941 (1988).
[8] M. Lindberg and S.W. Koch, Phys. Rev. B **38**, 7607 (1988).
[9] L. Allen and J.H. Eberly, *Optical Resonance and Two-Level Atoms* (Dover, New York, 1987).
[10] M. Joffre, D. Hulin, J. Foing, J. Chamberet, A. Migus, and A. Antonetti, IEEE J. Quantum Electron. **25**, 2505 (1989).
[11] M. Lindberg and S.W. Koch, Phys. Rev. B **38**, 3342 (1988).
[12] N. Sarakura, Y. Ishida, and H. Nakano, Opt. Lett. **16**, 153 (1991).
[13] W.H. Knox, D.S. Chemla, D.A.B. Miller, J.B. Stark, and S. Schmitt-Rink, Phys. Rev. Lett. **62**, 1189 (1989).
[14] J.H. Eberly and V.D. Popov, Phys. Rev. A **37**, 2012 (1988).
[15] M.G. Burt, Semicond. Sci. Technol. **5**, 1215 (1990).
[16] W.H. Knox, in *Hot Carriers in Semiconductor Nanostructures*, edited by J. Shah (Academic, New York, 1992).
[17] T. Tokizaki, Y. Ishida, and T. Yajima, Opt. Commun. **71**, 355 (1989).
[18] E.T.J. Nibbering, D.A. Wiersma, and K. Duppen, Phys. Rev. Lett. **68**, 514 (1992).
[19] M. Combescot, Phys. Rev. B **41**, 3517 (1990).
[20] M.D. Webb, S.T. Cundiff, and D.G. Steel, Phys. Rev. B **43**, 12 658 (1991).
[21] A.V. Kuznetsov, Phys. Rev. B **44**, 8721 (1991).
[22] A.V. Kuznetsov, Phys. Rev. B **44**, 13 381 (1991).